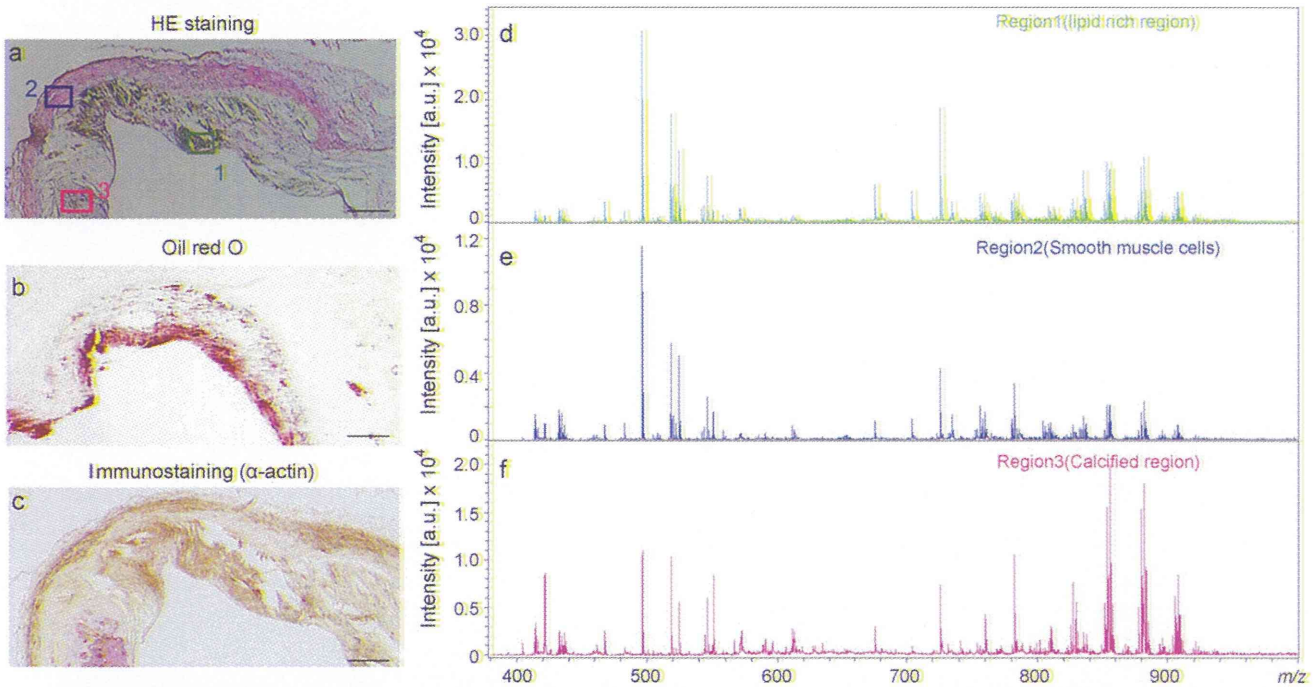

Fig. 1. The optical images and mass spectra of aortic root of ApoE-deficient mouse at 60 weeks of age. HE staining that has been stained after IMS (a). Scale bar: 100 μm. Region 1 is the lipid-rich region, region 2 is the SMCs, and region 3 is the calcified region. Oil red O staining (b). The immunostaining of α-actin, which is a marker for SMCs (c). The mass spectrum of region 1 (d), region 2 (e), and region 3 (f).

adventitia, which positively stained for the SMC marker α-actin (Fig. 1c). Region 3 is a calcified region in which chondrocytes were observed upon HE staining and immunostaining (Fig. 1a and c). Fig. 1d–f shows mass spectra obtained from all 3 regions. These mass spectra differ among the 3 regions, suggesting that a specific marker for each region could be found by comparing the 3 mass spectra.

We found 5 *m/z* values that were characteristic for the 3 regions. The molecules at *m/z* 671.6 and *m/z* 673.6 were specific for the lipid-rich region (Fig. 2a and b). These peaks were assigned as CE (18:2) and CE (18:1) on the basis of the *m/z* value. These 2 molecules showed the similar distribution. We made these images combine into a single color (Fig. 2c). The distribution of molecules at *m/z* 804.5 and *m/z* 832.5 were the same as the distribution of SMCs (Fig. 2d and e). The molecular ions at *m/z* 804.5 and 832.5 were assigned as PC (diacyl 16:0/20:4) and PC (diacyl 18:0/20:4) by MS/MS on tissue (Supplementary Fig. 1). PC was found to be dominantly detected as sodium adducted positive ion on the paraformaldehyde-fixed tissues (Supplementary Fig. 1). These 2 molecules showed the similar distribution. We made these images combine into a single color (Fig. 2f). We confirmed that the distribution of SMCs was not the same as the distribution of the other major PC species, such as PC (diacyl 16:0/16:0), PC (diacyl 16:0/18:0), PC (diacyl 16:0/18:1), PC (diacyl 16:0/18:2), PC (diacyl 18:0/18:0), PC (diacyl 18:0/18:1), and PC (diacyl 18:0/18:2) (Supplementary Fig. 2). The molecule at *m/z* 566.9 was specific for the calcified region (Fig. 2g). The monochrome image of *m/z* 566.9 is shown in Fig. 2h. The HE staining image and the merge image of each of the 3 regions are shown in Fig. 2i and j. These data indicated that we could distinguish the 3 regions by IbHE. The mass spectra of 3 regions are shown in Supplemental Fig. 3 and we confirmed that the distribution of other detected peaks in our experimental condition were different from 3 region (data not shown). Fig. 2k–m are images of aortic roots of ApoE deficient mice at 12 weeks of age. We used these aortic roots as non-atherosclerotic aortic roots because intimal thickening and lipid rich region were not observed in these samples (Fig. 2k and l). SMCs were observed in these samples (Fig. 2m). CE (18:2), CE (18:1), PC (diacyl 16:0/20:4), PC (diacyl 18:0/20:4) and *m/z* 566.9 were not detected by the analyses of these samples (Fig. 2n–p). These results suggest that CE (18:2), CE (18:1), PC (diacyl 16:0/20:4), PC (diacyl 18:0/20:4) and *m/z* 566.9 are the potential marker of atherosclerotic aortic roots of ApoE deficient mice. The identified potential marker list of aortic roots of the ApoE-deficient mice is summarized in Table 1.

We investigated whether the biomarkers of the mouse atherosclerotic aortae could be used to analyze the human atherosclerotic femoral arteries (Fig. 3). The distribution of CE (18:2) and CE (18:1) were partly the same as that of the oil red O positive region (Fig. 3a–d). The distribution of PC (diacyl 16:0/20:4) and PC (diacyl 18:0/20:4) were the same as the distribution of SMCs (Fig. 3e–h). The molecule at *m/z* 566.9 was not detected in the human samples (Fig. 3i–k). In the case of the human samples, the localization of the molecule at *m/z* 539.0 was the same as that of the calcified region (data not shown). The HE staining image and the merge image of the 3 regions are shown in Fig. 3l and m. We next investigated the distribution of lipid species because the distribution of CE was not completely the same as that of the region positively stained by oil red O staining. We found that there was TG (18:0/18:1/18:2) in the human atherosclerotic femoral arteries (Fig. 3o). The region where TG was detected was positively stained by oil red O staining (Fig. 3o ROI1). Adipocytes were not observed in the region where TG was detected. The characteristic distribution of TG (18:0/18:1/18:2) and CE is shown in Fig. 3q. The merge

Table 1
Identified potential marker list of mouse atherosclerotic lesion region.

Region	*m/z*	Assignment
Lipid rich region	671.6	CE (18:2)
	673.6	CE (18:1)
Smooth muscle cell	804.5	PC (diacyl 16:0/20:4)
	832.5	PC (diacyl 18:0/20:4)

Please cite this article in press as: Zaima N, et al. Imaging mass spectrometry-based histopathologic examination of atherosclerotic lesions. Atherosclerosis (2011), doi:10.1016/j.atherosclerosis.2011.03.044

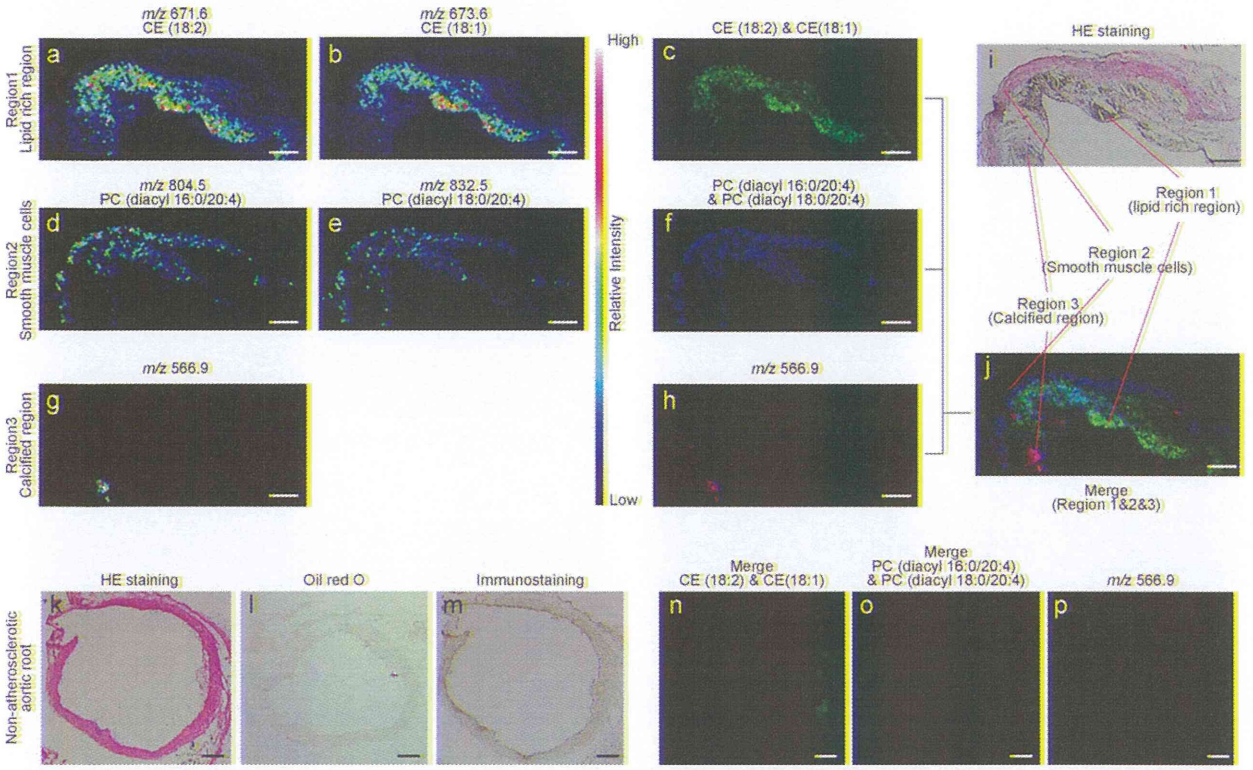

Fig. 2. The representative specific molecule images of a mouse atherosclerotic lesion. Scale bar: 100 μm. The specific ion images of region 1 (a and b) and the combined image of *m/z* 671.6 and 673.6 (c) ($n=3$). The specific ion images of region 2 (d and e) and the combined image of *m/z* 804.5 and 832.5 (f) ($n=3$). The specific ion images of region 3 (g) and the monochrome image of *m/z* 566.9 (h) ($n=3$). The comparison of HE staining (i) and the merge images of regions 1–3 (j). The image of non-atherosclerotic aortic roots of mice at 12 weeks of age ($n=3$) (k–m). Scale bar: 200 μm. HE staining that has been stained after IMS (k). Oil red O staining (l). The immunostaining of α-actin, which is a marker for SMCs (m). The merge image of CE (18:2) and CE (18:1) (n). The merge image of PC (diacyl 16:0/20:4) and PC (diacyl 18:0/20:4) (o). The ion image of *m/z* 566.9 (p).

image of TG and CE was the same as that of the oil red O positive stained region. The identified potential marker list for human atherosclerotic femoral arteries is summarized in Table 2.

4. Discussion

In this study, we were able to find and identify the characteristic molecules of atherosclerotic lesions in ApoE-deficient mice and humans, which indicated that our approach can be applied to the pathologic assessment of such lesions. Various cells and molecules that may be associated with plaque development and vulnerability are included in the atheroma. The mass spectra obtained from the lipid-rich region, the SMCs, and the calcified regions were different from each other (Fig. 1). This was because the mass spectra obtained by IMS reflected the profiles of their metabolites. We found specific molecules of atherosclerotic lesion of ApoE KO mouse (Fig. 2). The results obtained in Fig. 2 supported the existence of a real capacity of the spectra to differentiate between their pathologic conditions. CE (18:2) and CE (18:1) were specific for the lipid-rich regions of the mouse samples (Fig. 2a–c). These results were reasonable because CE was accumulated in the atherosclerotic plaque. PC (diacyl 16:0/20:4) and PC (diacyl 18:0/20:4) were found to be characteristic biomolecules of the SMCs in atherosclerotic lesions. It is of interest that the PCs that contain arachidonic acid (20:4) are the specific biomolecules of the SMCs. Arachidonic acid is a precursor of lipid mediators such as leukotriene (LT) and prostaglandin (PG), which induce inflammation [25]. The role of arachidonic acid in SMCs was not previously established. Therefore, it is of interest to clarify the role of PC (diacyl 16:0/20:4) and PC (diacyl 18:0/20:4) in SMCs. Because PC (diacyl 16:0/20:4) and PC (diacyl 18:0/20:4) were not detected in SMCs of non-atherosclerotic aortic roots of ApoE KO mice, we speculated PC (diacyl 16:0/20:4) and PC (diacyl 18:0/20:4) might play undesirable roles in the development of atherosclerotic lesions. The molecule at *m/z* 566.9 was specific for the calcified regions in our mice samples (Fig. 2g). We could not identify this molecule. In our opinion, this result does not compromise the intended histopathologic use of our approach, since the distinctions were valid even if the assignments were uncertain. However, further studies should be needed to identify the molecule at *m/z* 566.9 to enhance basic understanding of heart disease.

In the case of human atherosclerotic lesions, the distribution of PC (diacyl 16:0/20:4) and PC (diacyl 18:0/20:4) were the same as the distribution of SMCs (Fig. 3e–h). The specific biomolecules for the human calcified regions were not the same as those for the mouse calcified regions (Figs. 2J and 3m). This may be because the species differed or because there was a mature degree of calcification in the calcified regions. We found that CE and TG were localized in the lipid-rich regions of the human atherosclerotic lesions (Fig. 3o–q). Interestingly, the distributions of CE and TG were different from each another (Fig. 3q). TG was observed as intracellular

Table 2
Identified potential marker list of human atherosclerotic lesion region.

Region	*m/z*	Assignment
Lipid rich region	671.6	CE (18:2)
	673.6	CE (18:1)
	907.7	TG (18:0/18:1/18:2)
Smooth muscle cell	804.5	PC (diacyl 16:0/20:4)
	832.5	PC (diacyl 18:0/20:4)

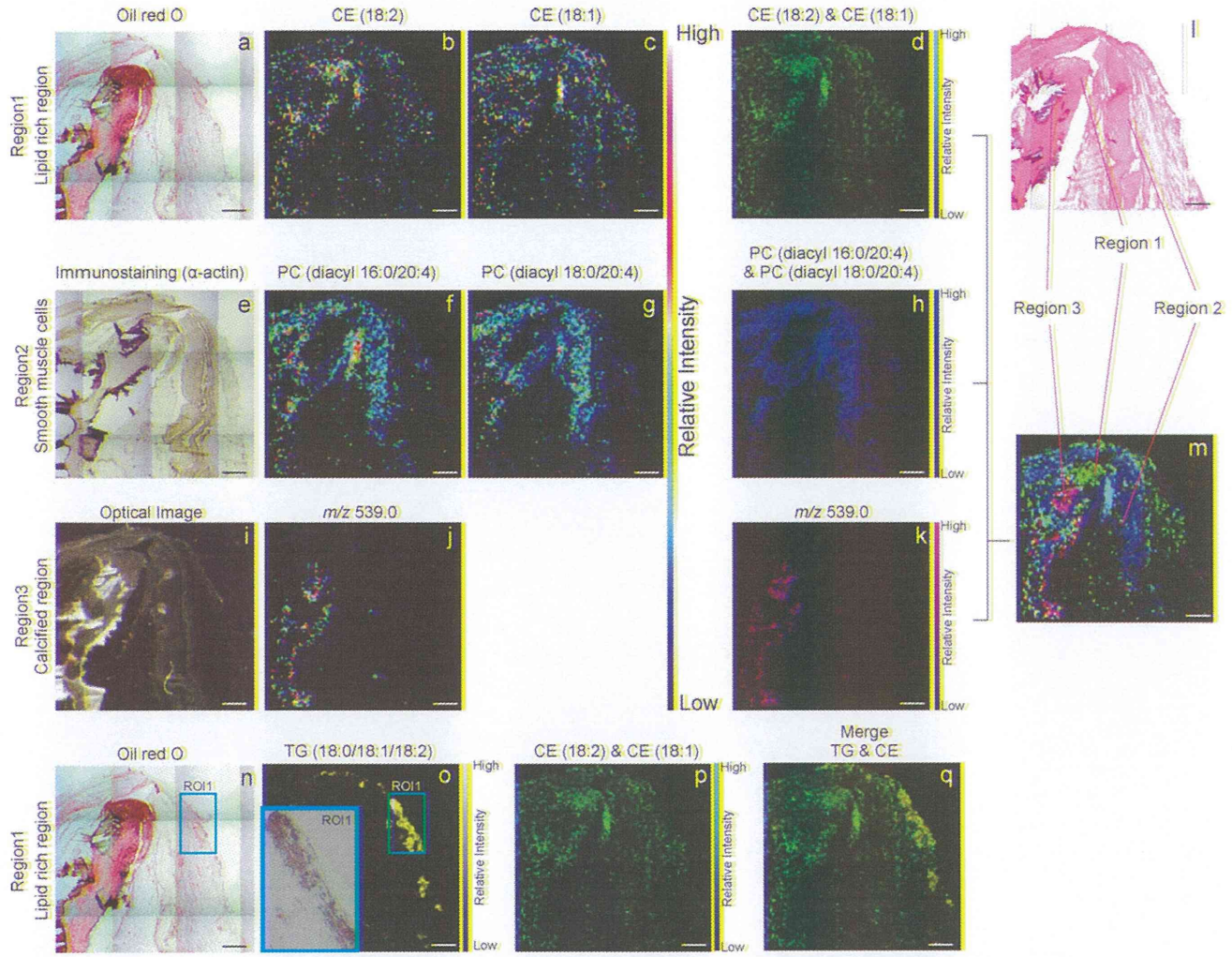

Fig. 3. The representative specific molecule images of a human atherosclerotic lesion ($n = 6$). Scale bar: 1000 μm. Oil red O staining (a and n). The ion images of CE (18:2) and CE (18:1) (b and c) and the combined monochrome images (d and p). The immunostaining of α-actin, which is a marker for SMCs (e). The ion images of PC (diacyl 16:0/20:4) and PC (diacyl 18:0/20:4) (f and g) and the combined monochrome images (h). The optical image of the analyzed sample (i). The ion image of m/z 539.0 (j) and the monochrome image (k). The comparison of HE staining (l) and the merge images of regions 1–3 (m). Consecutive sections are used in oil red O staining and immunostaining. The distribution of TG (18:0/18:1/18:2) (o). ROI1: high power field of oil red O staining. The merge image of TG and CE (q).

lipid droplets (Fig. 3o ROI1). Although the role of TG in the evolution of atherosclerosis remains unknown, there is a possibility that TG plays an important role in the evolution of atherosclerosis, as we previously found the characteristic phenotype that accumulates TG in aortic atherosclerotic lesions, while accumulated cholesterol level was normal [9]. It is reported that EPA ethyl ester, which is a drug used to reduce serum TG levels, decreases the incidence of coronary events in hypercholesterolemia with impaired glucose metabolism [26]. The mechanism of action of EPA ethyl ester may be involved in the TG in atherosclerotic lesions. The reanalysis of human atherosclerotic lesions by IbHE may be an important way to clarify the role of TG in the development of atherosclerosis.

5. Conclusion

We detected specific molecular markers for atherosclerotic lesions in ApoE-deficient mice and in humans by using IbHE, indicating that specific peaks can be likened to antigens in immunostaining. Because IMS can detect numerous peaks that reflect the metabolic profile of optional regions (Fig. 1d–f), several characteristic peaks of the regions of interest can be identified. Therefore, this approach conceptually distinguishes all atherosclerotic components on basis of the combination of characteristic peaks. Since many factors are involved in the development of atherosclerosis [27–29], a larger-scale study to identify the specific molecules of other atherosclerotic lesion components, such as leukocytes, is necessary. In addition, a reexamination of vascular disease by IbHE might elucidate new findings, because IbHE can visualize the localization of low molecular weight molecules, which are rarely visualized by other techniques. At this time, IMS is the only method for the specific and simultaneous visualization of lipids in tissue sections. Lipids are considered strong risk factors for atherosclerosis. Therefore, many clinical trials specifically targeted serum lipid control in order to develop treatments for atherosclerotic diseases. We speculate that the accumulated lipids in atherosclerotic lesions do not belong to a single lipid species such as CE. Determining the localization and class of lipids in atherosclerotic lesions by using IbHE can be an important tool for the pathologic analysis of such lesions. One limitation of our approach is spatial resolution. The spatial resolution of IMS is limited to >10 μm at this time [30]. Therefore, a combination of

Please cite this article in press as: Zaima N, et al. Imaging mass spectrometry-based histopathologic examination of atherosclerotic lesions. Atherosclerosis (2011), doi:10.1016/j.atherosclerosis.2011.03.044

conventional staining and IbHE is essential for a successful micron-order analysis.

Disclosures

We have no potential conflicts of interest to report for any of the funding listed above. We include 2 tables and 3 figures in the paper (3 figures destined to on line only supplementary material).

Sources of funding

This work was supported by the Program for Promotion of Basic and Applied Researches for Innovations in Bio-oriented Industry (BRAIN) and a Grant-in-Aid for Scientific Research (C) (22590522) to N.Z.

Acknowledgment

We would like to thank Mayumi Suzuki for her technical assistance.

Appendix A. Supplementary data

Supplementary data associated with this article can be found, in the online version, at doi:10.1016/j.atherosclerosis.2011.03.044.

References

[1] Weber C, Zernecke A, Libby P. The multifaceted contributions of leukocyte subsets to atherosclerosis: lessons from mouse models. Nat Rev Immunol 2008;8:802–15.
[2] Hansson GK. Inflammation, atherosclerosis, and coronary artery disease. N Engl J Med 2005;352:1685–95.
[3] Doran AC, Meller N, McNamara CA. Role of smooth muscle cells in the initiation and early progression of atherosclerosis. Arterioscler Thromb Vasc Biol 2008;28:812–9.
[4] Virmani R, Burke AP, Farb A, Kolodgie FD. Pathology of the vulnerable plaque. J Am Coll Cardiol 2006;47:C13–8.
[5] Tabas I. Macrophage apoptosis in atherosclerosis: consequences on plaque progression and the role of endoplasmic reticulum stress. Antioxid Redox Signal 2009;11:2333–9.
[6] Aikawa M, Libby P. The vulnerable atherosclerotic plaque: pathogenesis and therapeutic approach. Cardiovasc Pathol 2004;13:125–38.
[7] Ross R. Atherosclerosis—an inflammatory disease. N Engl J Med 1999;340:115–26.
[8] Goldstein JL, Brown MS. Familial hypercholesterolemia: identification of a defect in the regulation of 3-hydroxy-3-methylglutaryl coenzyme a reductase activity associated with overproduction of cholesterol. Proc Natl Acad Sci USA 1973;70:2804–8.
[9] Hirano K, Ikeda Y, Zaima N, Sakata Y, Matsumiya G. Triglyceride deposit cardiomyovasculopathy. N Engl J Med 2008;359:2396–8.
[10] Cornett DS, Reyzer ML, Chaurand P, Caprioli RM. Maldi imaging mass spectrometry: molecular snapshots of biochemical systems. Nat Methods 2007;4:828–33.
[11] Zaima N, Hayasaka T, Goto-Inoue N, Setou M. Matrix-assisted laser desorption/ionization imaging mass spectrometry. Int J Mol Sci 2010;11:5041–56.
[12] Touboul D, Piednoel H, Voisin V, et al. Changes of phospholipid composition within the dystrophic muscle by matrix-assisted laser desorption/ionization mass spectrometry and mass spectrometry imaging. Eur J Mass Spectrom (Chichester, Eng) 2004;10:657–64.
[13] Hayasaka T, Goto-Inoue N, Sugiura Y, et al. Matrix-assisted laser desorption/ionization quadrupole ion trap time-of-flight (Maldi-Qit-Tof)-based imaging mass spectrometry reveals a layered distribution of phospholipid molecular species in the mouse retina. Rapid Commun Mass Spectrom 2008;22:3415–26.
[14] Murphy RC, Hankin JA, Barkley RM. Imaging of lipid species by Maldi mass spectrometry. J Lipid Res 2009;50:S317–22.
[15] Zaima N, Goto-Inoue N, Adachi K, Setou M. Selective analysis of lipids by thin-layer chromatography blot matrix-assisted laser desorption/ionization imaging mass spectrometry. J Oleo Sci 2011;60:93–8.
[16] Zaima N, Matsuyama Y, Setou M. Principal component analysis of direct matrix-assisted laser desorption/ionization mass spectrometric data related to metabolites of fatty liver. J Oleo Sci 2009;58:267–73.
[17] Goto-Inoue N, Hayasaka T, Zaima N, Setou M. The specific localization of seminolipid molecular species on mouse testis during testicular maturation revealed by imaging mass spectrometry. Glycobiology 2009;19:950–7.
[18] Colsch B, Woods AS. Localization and imaging of sialylated glycosphingolipids in brain tissue sections by Maldi mass spectrometry. Glycobiology 2010;20:661–7.
[19] Groseclose MR, Andersson M, Hardesty WM, Caprioli RM. Identification of proteins directly from tissue: in situ tryptic digestions coupled with imaging mass spectrometry. J Mass Spectrom 2007;42:254–62.
[20] Stoeckli M, Chaurand P, Hallahan DE, Caprioli RM. Imaging mass spectrometry: a new technology for the analysis of protein expression in mammalian tissues. Nat Med 2001;7:493–6.
[21] Goto-Inoue N, Setou M, Zaima N. Visualization of spatial distribution of gamma-aminobutyric acid in eggplant (*Solanum Melongena*) by matrix-assisted laser desorption/ionization imaging mass spectrometry. Anal Sci 2010;26:821–5.
[22] Zaima N, Goto-Inoue N, Hayasaka T, Setou M. Application of imaging mass spectrometry for the analysis of Oryza Sativa rice. Rapid Commun Mass Spectrom 2010;24:2723–9.
[23] Zaima N, Hayasaka T, Goto-Inoue N, Setou M. Imaging of metabolites by Maldi mass spectrometry. J Oleo Sci 2009;58:415–9.
[24] Hayasaka T, Goto-Inoue N, Zaima N, Kimura Y, Setou M. Organ-specific distributions of lysophosphatidylcholine and triacylglycerol in mouse embryo. Lipids 2009;44:837–48.
[25] Kuehl Jr FA, Egan RW. Prostaglandins, arachidonic acid, and inflammation. Science 1980;210:978–84.
[26] Oikawa S, Yokoyama M, Origasa H, et al. Suppressive effect of epa on the incidence of coronary events in hypercholesterolemia with impaired glucose metabolism: sub-analysis of the Japan Epa lipid intervention study (Jelis). Atherosclerosis 2009;206:535–9.
[27] Laxton RC, Hu Y, Duchene J, et al. A role of matrix metalloproteinase-8 in atherosclerosis. Circ Res 2009;105:921–9.
[28] Zakkar M, Chaudhury H, Sandvik G, et al. Increased endothelial mitogen-activated protein kinase phosphatase-1 expression suppresses proinflammatory activation at sites that are resistant to atherosclerosis. Circ Res 2008;103:726–32.
[29] Paulson KE, Zhu SN, Chen M, et al. Resident intimal dendritic cells accumulate lipid and contribute to the initiation of atherosclerosis. Circ Res 2010;106:383–90.
[30] Harada T, Yuba-Kubo A, Sugiura Y, et al. Visualization of volatile substances in different organelles with an atmospheric-pressure mass microscope. Anal Chem 2009;81:9153–7.

Please cite this article in press as: Zaima N, et al. Imaging mass spectrometry-based histopathologic examination of atherosclerotic lesions. Atherosclerosis (2011), doi:10.1016/j.atherosclerosis.2011.03.044

Anal Bioanal Chem (2012) 403:1775–1776
DOI 10.1007/s00216-012-5922-x

EDITORIAL

Biomedical mass spectrometry

Toyofumi Nakanishi · Mitsutoshi Setou · Tomiko Kuhara

Published online: 10 April 2012

The 36th Annual Meeting of the Japanese Society for Biomedical Mass Spectrometry (JSBMS) was held on September 15 and 16, 2011, in the Galaxy Hole Room in Hotel Hankyu Expo Park, Osaka, Japan. The theme of the meeting was "New challenges not for clinical research but for medical services: from mass profiling to mass imaging " and covered a variety of biomedical applications, such as diagnosis and disease state assessment of inherited metabolic disorders, forensic toxicological analysis, proteomics, metabolomics, and imaging mass spectrometry. At this meeting, we partially collaborated with the Japan Society of Mass Spectrometry (JSMS) during the invited sessions on the first day.

On the first day, there was joint program with the JSMS in the afternoon session. We invited four famous researchers: Prof. Shu-ichi Ikeda from Shinshu University (School of Medicine)—he presented a lecture entitled "Pathogenesis and therapeutic approaches in systemic amyloidosis"; Dr. Pierre Chaurand from Montreal University (Department of Chemistry)—he presented a lecture entitled "Imaging mass spectrometry: current performances and upcoming

Published in the special paper collection *Biomedical Mass Spectrometry* with guest editors Toyofumi Nakanishi and Mitsutoshi Setou.

T. Nakanishi (✉)
Clinical and Laboratory Medicine, Osaka Medical College,
2-7 Daigaku-cho,
Takatsuki, Osaka 569-8686, Japan
e-mail: nakanisi@poh.osaka-med.ac.jp

M. Setou
Department of Cell Biology and Anatomy,
Hamamatsu University School of Medicine,
1-20-1 Handayama,
Hamamatsu, Shizuoka 431-3192, Japan

T. Kuhara
Division of Human Genetics, Medical Research Institute,
Kanazawa Medical University,
Uchinada-machi,
Kahoku-gun, Ishikawa 920-0293, Japan

Toyofumi Nakanishi is an associate professor of clinical and laboratory medicine at Osaka Medical College. His research interests include clinical application of imaging mass spectrometry and clinical diagnosis of soft-ionization mass spectrometry coupled with immunoprecipitation. He is the author of 65 peer-reviewed papers, 35 scientific papers, and 13 book chapters.

Mitsutoshi Setou has been a full professor of anatomy and cell biology at the Hamamatsu University School of Medicine since 2008. His research interests include development and application of imaging mass spectrometry and systems biology with "omics" technologies. He is the author of over 100 peer-reviewed papers, 150 scientific papers, and ten book chapters, and is the editor of a book on imaging mass spectrometry.

Tomiko Kuhara, president of JSBMS from 2007 to 2011, is a professor of human genetics at Kanazawa Medical University. Her research interests have included the development and application of metabolic profiling based on gas chromatography/mass spectrometry since the 1970s and metabolomic profiling since the early 1990s. The diagnostic procedures she has developed are extremely useful for noninvasive differential chemical diagnosis of around 130 disease conditions (including more than 100 inherited metabolic disorders) and for personalized medicine. The procedures are also very effective for all stages of drug R & D.

challenges"; Dr. Yoshinao Wada, General Director of the Osaka Prefectural Research Institute for Maternal and Child Health—he presented a lecture entitled "Past and future trends of biomedical applications: measuring quality or quantity"; and Prof. Frantisek Turecek from Washington University (Department of Chemistry)—he presented a lecture entitled "Tandem mass spectrometry and clinical enzymology: toward newborn screening of lysosomal storage disorders." Also, on the same day, three young scientists (Dr. Daisuke Saegusa from Tohoku University, Dr. Ikuko Yao from Kansai Medical University, and Dr. Mototada Hichiri from the National Institute of AIST) won the awards for the best poster presentations. There was a symposium on forensic and toxicological mass spectrometry, organized by Dr. Hitoshi Tsuchihashi from Osaka Medical College. In this session, a surprise guest presented a lecture entitled "Drug history in a longitudinally sliced hair section by MALDI imaging." The group concerned were the first to demonstrate the traceability of drug history every few hours using only a sliced hair section (*J. Mass Spectrom.* 46:411-416, 2011).

On the second day, there were two symposia, entitled "New applications to clinical microbiology by mass spectrometry," organized by Prof. Fumio Nomura from Chiba University, and "Developments of imaging mass spectrometry," organized by Prof. Mitsutoshi Setou from Hamamatsu Medical University. In workshops I and II, there were technical sessions. One was entitled "Current MS technology and its associate techniques," organized by Prof. Shigeo Ikegawa from Kinki University and Prof. Kuniaki Saito from Kyoto University. The other was entitled "Applications of MS techniques: questions and answers for good-quality MS data," organized by Dr. Takeshi Kasama from Tokyo Medical and Dental University and Toshie Takahashi from Tokyo University.

This special issue is based on the presentations at the 36th Annual Meeting of JSBMS in Osaka Senri. There were 23 oral presentations (three regular sessions, three symposia, and four invited lectures), 36 poster presentations, and 202 participants at this meeting (see Fig. 1). We would like to thank all speakers, presenters, participants, and staff members for the excellent papers, earnest discussion, and cooperation at this fruitful meeting.

Fig. 1 Participants of the 36th Annual Meeting of the Japanese Society for Biomedical Mass Spectrometry in Osaka Senri

Current Topics

Challenge of Mass Spectrometry toward the Elucidation of Life Phenomena

Development of Imaging Mass Spectrometry

Yusuke Saito, Michihiko Waki, Saira Hameed, Takahiro Hayasaka, and Mitsutoshi Setou*

Department of Cell Biology and Anatomy, Hamamatsu University School of Medicine; 1–20–1 Handayama, Higashi-ku, Hamamatsu, Shizuoka 431–3192, Japan.

Received February 3, 2012

We have developed a mass microscope in which a microscope is combined with high-resolution matrix assisted laser desorption/ionization-imaging mass spectrometry (MALDI-IMS). This technique is a powerful tool for investigating the spatial distribution of biomolecules without the need for any time-consuming extraction, purification, and labeling procedures for biological tissue sections. The mass microscope provides clear images with regards to the distribution of hundreds of biomolecules in a single measurement, and also helps in determining the cellular profile of the biological system. In this review, we focus on some of the recent developments in clinical applications and describe how the mass microscope can be employed to assess pathomorphology and pharmacokinetics.

Key words imaging; mass spectrometry; microscopy; analytical biochemistry; drug kinetics

1. INTRODUCTION

Imaging is a technique that can be used to visualize cellular and molecular processes that occur in living organisms in a two-dimensional (2-D) or three-dimensional (3-D) fashion, without perturbing the structure of the system. The various techniques currently available include X-rays,[1] nuclear magnetic resonance,[2] cryo-electron microscopes,[3] positron emission tomography,[4] immunohistochemistry,[5–8] green fluorescent protein labeling,[9–12] and luciferase.[13] The green fluorescent protein labeling technique involves over expression of the fusion protein of the concerned molecule and green fluorescent protein.[12,14] However, these techniques can only provide information on the structure of the material. There is also a "nonlabeling" technique even at the electron microscopic level,[3] and yet there is still a serious limitation on the object preference. Imaging mass spectrometry (IMS)[15] is an emerging technique that is expected to at once resolve these problems in conventional morphological examinations. In IMS, mass spectra associated with spatial information can be simultaneously recorded to obtain expression patterns of various molecules in specimens to be analyzed. This new generation of mass spectrometry (MS) has been used for the analysis of biological compounds at either the tissue[16–19] or single-cell level.[20–23] Recent IMS studies have been conducted on a variety of topics, including biological applications[24–30] and pathological applications.[31,32] In addition to the analysis of protein described in the above references, direct lipid analysis in mammalian tissues[33,34] has also been conducted, and histopathological materials[35] and pharmacokinetics in rat whole body sections[36] have been studied.

IMS can be used to visualize the spatial distribution of biomolecules based on the mass-to-charge ratio (m/z) of the target molecule in the mass spectrum. Several ionization methods, such as desorption electrospray ionization (DESI),[37] secondary ion mass spectrometry (SIMS),[38] and matrix-assisted laser desorption/ionization (MALDI) have been investigated.[39] DESI is an ionization technique by which the molecules are ionized without addition of organic matrix under ambient conditions. In this method, the surface of the sample is analyzed by charged droplets of solvent, generated during the electrospraying. DESI has a limited spatial resolution of 0.3–0.5 mm, which is not a sufficiently high resolution for imaging. SIMS on the ion microprobe offers the best combination of spatial resolution (20 μm beam diameter) and precision (0.2 per mL for sulfur isotopes). This technique is applicable for the analysis of small molecules (<1 kDa) because the high energy of the SIMS causes the fragmentation of larger molecules. On the other hand, MALDI is used to visualize biomolecules such as lipids less than 1 kDa as well as peptides and proteins over 10 kDa.

MALDI-IMS is a powerful tool that allows the simultaneous mapping of hundreds of molecules in a tissue section in a single measurement. To use a mass spectrometer as an imaging instrument, it is essential for the spectrometer to be equipped with an automatic rastering function, automatic data acquisition system, and visualization software. Recently, several manufacturers have released novel instruments having these features. Almost all manufacturers have developed in-house software for their instruments and have included a driver for instrument and image reconstruction. On the other hand, the user-friendly visualization software BioMap[40] is freely available; it is used commonly in mass imaging (MALDI MSI HP, http://www.maldi-msi.org/content).

Our group has developed the original equipment in collaboration with Shimadzu Corporation of Japan and extended the techniques for molecular profiling of different tissue samples, such as brain,[41–43] liver,[44] testis,[45] and retina[46] of mice, and colon cancer in human,[47] involving sample preparation,[25,48–50] and the nanoparticle-based ionization process in IMS.[51–53] In

* To whom correspondence should be addressed. e-mail: setou@hama-med.ac.jp

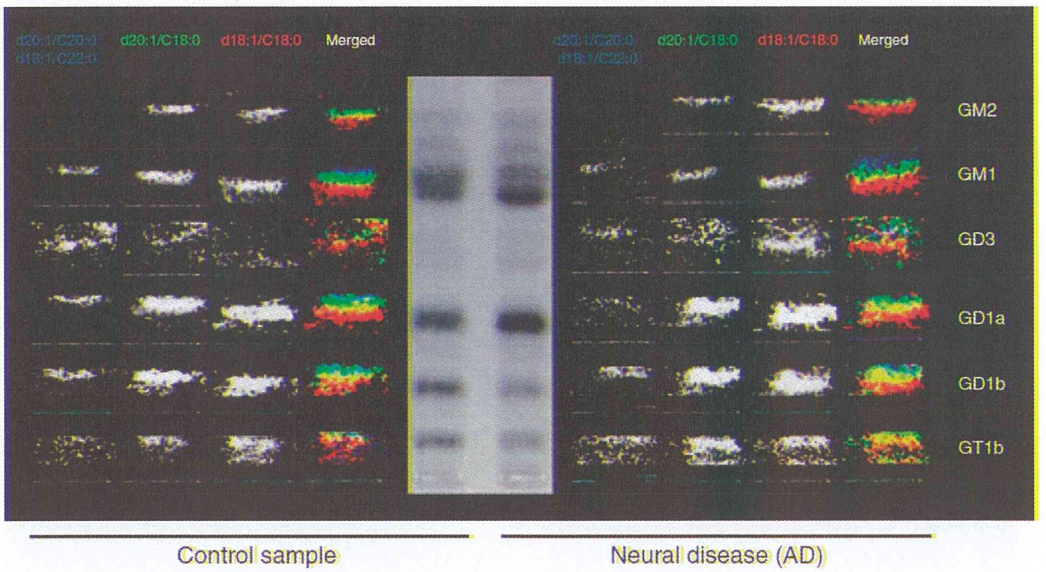

Fig. 1. TLC-Blot-MALDI-QIT-TOF-MS Imaging of Hippocampus Gray Matter Gangliosides

The raster scan of the polyvinylidene difluoride membrane was performed automatically. The number of laser irradiations was 5 shots in each spot. The interval of data points was 200 lm. The color red indicates a d18:1 sphingosine-containing signal, the color green a d20:1 sphingosine-containing signal, and the color blue a d18:1/C22:0- or d20:1/C20:0-containing signal. Merged images of these are shown on the right side of each panel. (Reprinted from ref. 60 with permission from Blackwell Publishing.)

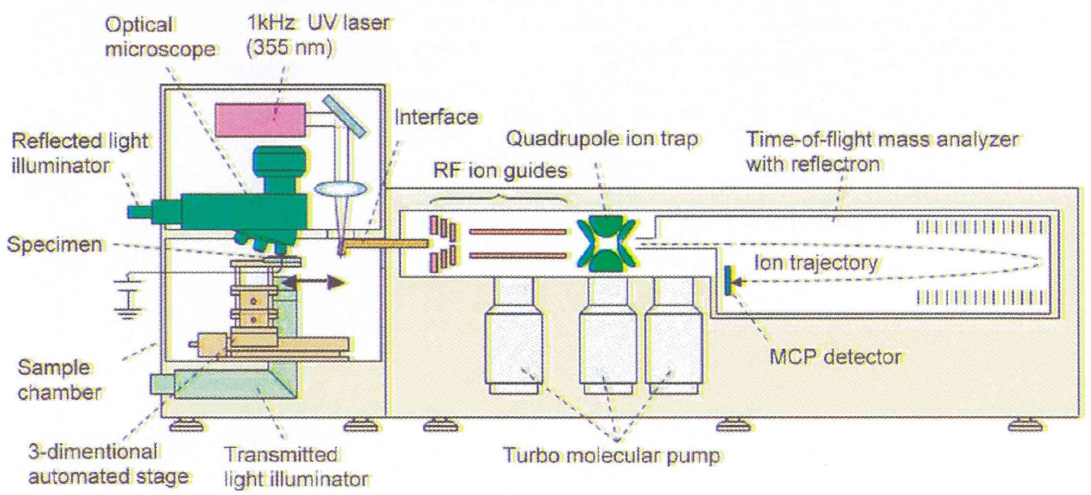

Fig. 2. Schematic Diagram Showing the Mass Microscope

(Reprinted from ref. 66 with permission from the American Chemical Society.)

recent years, MALDI imaging has resulted in many developments for assessing the localization of molecular species in biological samples. Several applications represent the direct entailment of this technology to basic clinical research. Here, we discuss the recent developments concerning MALDI-IMS.

2. TARGETS OF ANALYSIS BY MALDI-IMS

2.1. Imaging of Glycosphingolipids Glycosphingolipids (GSLs) play important roles in various brain functions. To investigate the mechanisms of brain function in more detail, it is necessary to understand the composition and function of GSLs. We have studied GSLs in previous research.[6,14,54,55] Thin-layer chromatography (TLC) is routinely used for the separation and partial characterization of neutral and acidic GSLs and phospholipids in mixtures.[56–58] However, even under optimized TLC conditions, TLC characterization of individual GSLs does not yield unambiguous structural information. Information regarding the compositions of these highly complex mixtures remains limited. The same sugar moiety in different GSLs may migrate to different positions owing to differences in their ceramide structures. Multi-stage MS (MS^n) analysis can supply information on each ceramide structure. However, it is difficult to identify individual molecular species by MS alone. Therefore, by combining TLC and MS, we were able to obtain a complete set of information on GSLs.

Our group has used MALDI-MS/MS to study colon cancer liver metastasis in 3 μm thick tissue sections. MS/MS investigations of normal and cancerous cells revealed

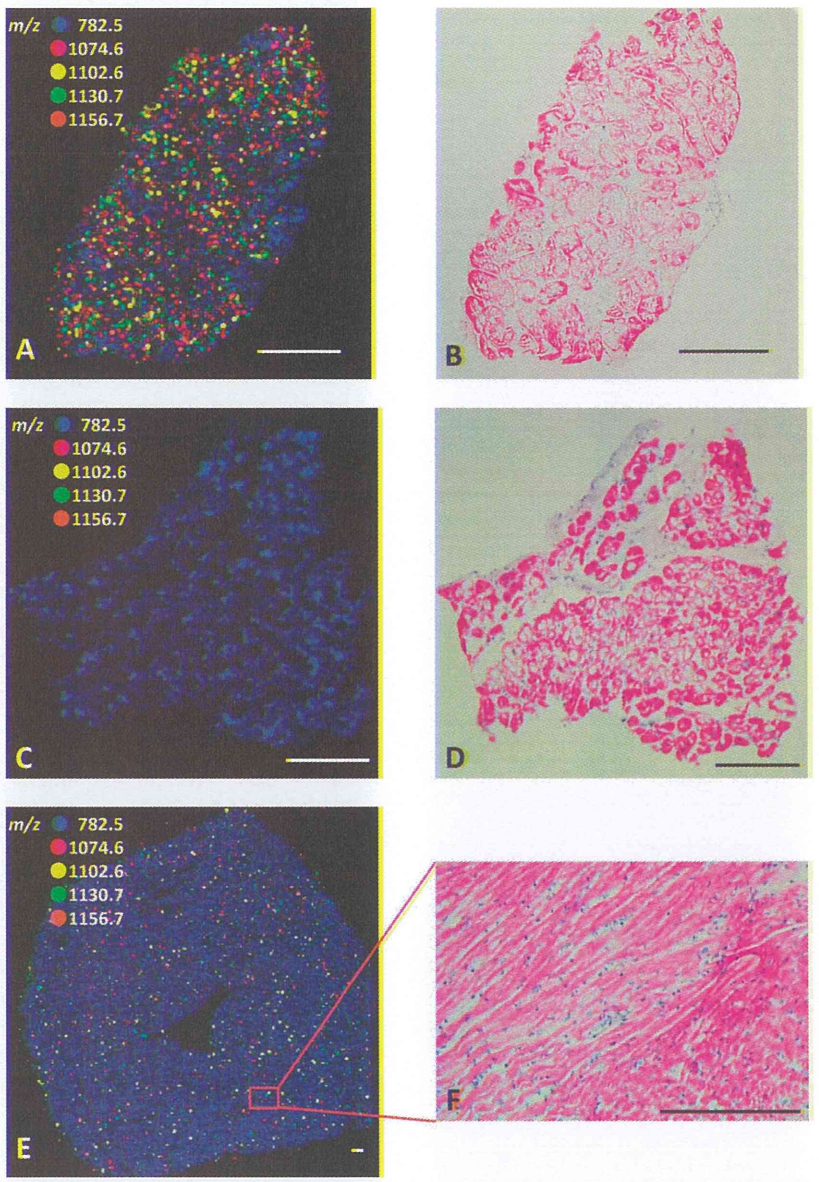

Fig. 3. IMS and Histology of the Samples

We constructed a figure by plotting the positions of the *m/z* 782.5, 1074.6, 1102.6, 1130.7 and 1156.7 peaks. When we compared (A) IMS with (B) a hematoxylin and eosin-stained section, the peaks of Gb3s were more densely packed in cardiomyocytes with vacuolar degeneration, and the Gb3s existed together in some parts and separately in others. (C,D) In contrast, Gb3 was not detected in a control sample from a patient with secondary myocardial degenerative changes with aortic regurgitation. (E,F) Gb3s were also detected on IMS in the heart of a mouse with Fabry's disease even though there was no evidence of vacuolar changes in the myocardium on light microscopy. Bar, 200 μm. (Reprinted from ref. 67 from Official Journal of the Japanese Circulation Society.)

that the cancerous cells accumulated sphingomyelin.[47] We have also studied the localization of seminolipids in mouse testis during testicular maturation, and the organ-specific distribution of lysophosphotidylcholine and triacylglycerol in mouse embryos using IMS.[45,59] Recently, our group has developed a TLC-Blot-MALDI-TOF-IMS system which can separate and partially characterize acidic and neutral GSLs. Here, we describe gangliosides identified from a control patient and a patient with Alzheimer's disease using TLC-Blot-MALDI-TOF-MS imaging of the hippocampus gray matter (Fig. 1). In the Alzheimer's patient, the GM2 and GD3 ganglioside bands appeared to be clearer than those of the control. The relative increases in d18:1 sphingosine-containing gangliosides in the patient with Alzheimer's disease are also expressed in this image.[60]

2.2. Imaging of Proteins and Peptides Immunohistochemistry has been commonly used for profiling protein distribution in tissue sections. In this approach, antibodies are needed to detect specific proteins. Other genomic and proteomic approaches cannot be applied to biopsies as the quantity of sample available is only very small.[14,61–63] Our group has analyzed *SCRAPPER* (A protein we first reported that is localized in neuronal synapses.)[6] knockout mouse by utilizing a proteomic approach based on an IMS technique.[64] We have also demonstrated that the denaturation process and detergent-supplemented trypsin solution can improve the protein digestion efficiency for direct tissue analysis with IMS.[65] We recently developed a formalin-fixed paraffin-embedded

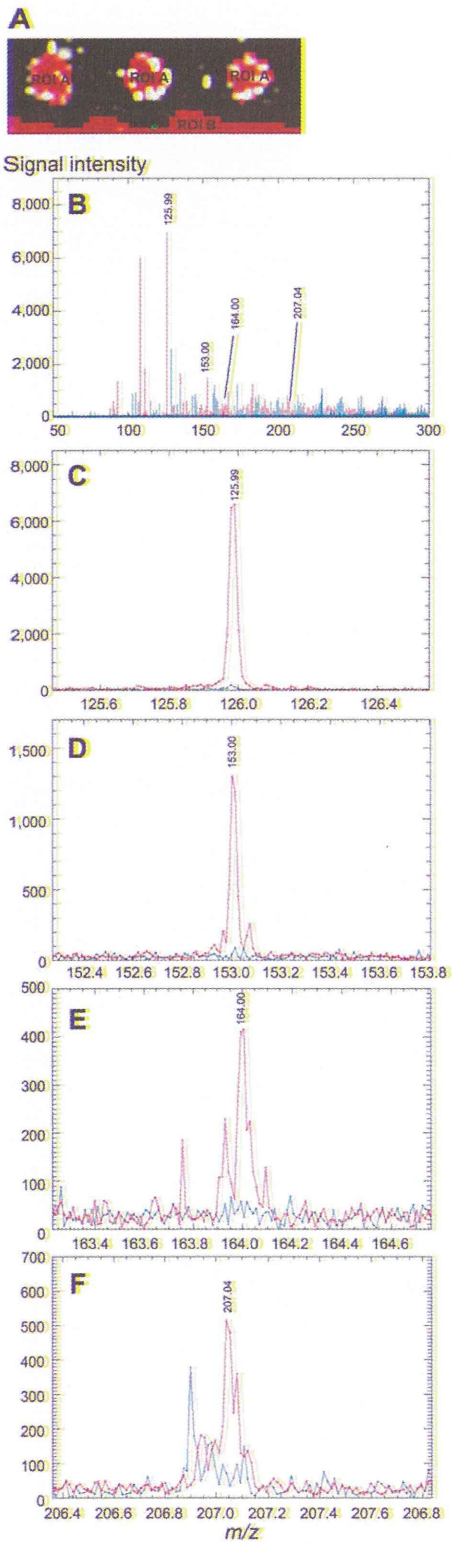

Fig. 4. Hair-Specific Mass Spectra of Putative Aging Markers

ROI-specific mass spectra in subject No. 1 are presented. Red peaks and blue peaks are derived from the hair section and background area, respectively. (A) ROI selection is illustrated: ROI A as hair section and ROI B as background area. (B) *m/z* 50 to 300. (C) *m/z* 125.99. (D) *m/z* 153.00. (E) *m/z* 164.00. (F) *m/z* 207.04. (Reprinted from ref. 68 with permission from The Public Library of Science.)

tissue microarray to study gastric carcinoma tissue samples by IMS, and successfully identified histone (H4)-specific signals in poorly differentiated cancer tissue samples by utilizing tandem MS.[63] Proteomic-based IMS investigations have resulted in a better understanding of carcinogenesis, invasiveness, metastasis, and the prognosis process in gastric cancer patients.

3. DEVELOPMENT AND APPLICATION OF HIGH-RESOLUTION ATMOSPHERIC PRESSURE-LASER MASS MICROSCOPE

3.1. Development of a 'Mass Microscope' Recently, we have developed a 'mass microscope' consisting of a microscope coupled with high-resolution atmospheric pressure-laser desorption/ionization (AP-LDI) and a quadruple ion trap-time-of-flight (QIT-TOF)-analyzer[66] (Fig. 2). This instrument allows us to precisely observe a specific tissue section before IMS and analyze the biomolecules with a spatial resolution of 10 μm on the tissue section. An UV laser tightly focused with a triplet lens was used to achieve high spatial resolution. An atmospheric pressure ion-source chamber enables us to analyze fresh samples with minimal loss of intrinsic water or volatile compounds.

3.2. Analysis of Disease Biomarkers in Fabry's Disease We have used IMS to achieve the accurate diagnosis of Fabry's disease, especially in questionable cases, and have shown that IMS has a higher specificity than electron microscopy or enzyme activity assays, which are based on light microscopy. We constructed images by determining the locations of these peaks within an endomyocardial (EMB) biopsy sample.[67] We observed that the distribution of globotriaosylceramides (Gb3s) was consistent with that of cardiomyocytes, especially in areas that were affected by vacuolar degeneration, and that the Gb3 types existed together in some parts and separately in others (Figs. 3A, B). In contrast, as shown in Figs. 3C and D, Gb3 was not detected in the control EMB sample. When we analyzed the heart from a mouse with Fabry's disease, we also detected Gb3s in the cardiac tissue, even though there was no evidence of vacuolation in the cardiomyocytes on light microscopy (Figs. 3E, F). Gb3 was not detected in the control mouse heart. We could detect Gb3s not only in the heart from a Fabry's disease patient, but also in the heart from a mouse model of Fabry's disease without discernible degenerative changes on light microscopy. Although the significance of each type of Gb3 distribution is unknown, it is possible that these distribution patterns could help to distinguish variations in the disease phenotype or evaluate the effectiveness of enzyme replacement therapy, which may also help to elucidate the basis for the disease. However, this issue requires further study. The current study presents novel findings suggesting that IMS is useful for diagnosing Fabry's disease with cardiac manifestations, especially in questionable cases. Because IMS can directly analyze the molecular weight of each existing component, IMS has a higher specificity than electron microscopy or enzyme activity assays when Fabry's disease is suspected based on light microscopy. Our results indicate that IMS is a new tool that can be used to accurately diagnose not only Fabry's disease, but also other unknown storage diseases.

3.3. Analysis of Biomolecules in Human Hair The mass microscope has a subcellular spatial resolution of 10 μm for the detection of molecules from a tissue section. We have